The ITB Journal

Volume 6 | Issue 1 Article 1

2005

An Introduction to the Quasi-Optical Design of the HIFI Instrument for the Herschel Space Observatory

Gareth S. Curran

J. Anthony Murphy

An Introduction to the Quasi-Optical Design of the HIFI Instrument for the Herschel Space Observatory

Gareth S. Curran[1], J. Anthony Murphy[2]

1. School of Informatics and Engineering, Institute of Technology, Blanchardstown
2. Department of Experimental Physics, National University of Ireland, Maynooth

Abstract

This paper is concerned with the quasi-optical design and analysis of the Heterodyne Instrument for the Far Infrared (HIFI) on board the European Space Agency's Herschel Space Observatory, which is due for launch in 2007. The paper begins with an introduction to astronomy at submillimetre wavelengths followed by the science that will be carried out by HIFI. The optical layout of HIFI is presented and the quasi-optical techniques used in the analysis of band 5 of the instrument are discussed, in particular, issues associated with the design and performance of the integrated lens antenna for this band. A power coupling efficiency calculation is carried out and the overall performance of the telescope is analysed.

1. Introduction

The Herschel Space Observatory is named after Sir Frederick William Herschel (1738 – 1822) who is, in a sense, the father of infrared astronomy (although he is probably most famous for his discovery of the planet Uranus in 1781). Herschel discovered the non-visible part of the electromagnetic spectrum while trying to determine whether different colours of light contained different amounts of heat by using a thermometer and a prism to disperse sunlight. To his surprise, he found that the region just beyond the red light seemed to have the highest temperature of all, a region supposedly devoid of sunlight.

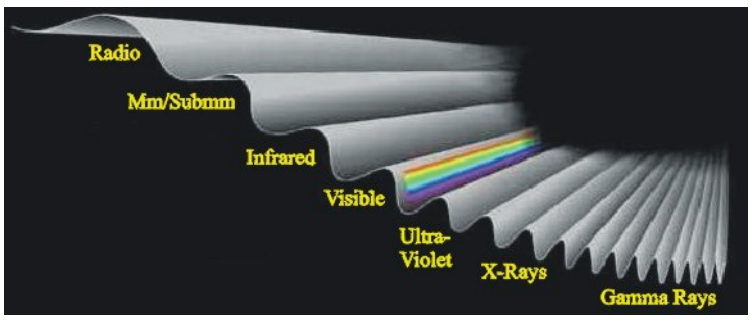

Fig. 1.1: Schematic diagram of the electromagnetic spectrum.

It is now known that the electromagnetic spectrum extends from long wavelength radio waves (λ~20m) to extremely high-energy gamma rays (λ~10^{-6}nm), as illustrated in Fig.1.1. The

visible region of the spectrum is very narrow ranging from 400nm to 700nm. The millimetre and submillimetre region, in which this paper concentrates, lies between the radio and infrared wavelengths. Strictly speaking, submillimetre refers to electromagnetic emissions at frequencies in the range of 300GHz to 1000GHz. The term *terrahertz* is now used to refer to frequencies greater than 1000GHz.

In 1932, Karl Jansky detected radio emissions from our own galaxy, the Milky Way [14]. This new phenomenon of observing non-visible radiation from space created a whole new branch of astronomy. Previously unseen objects in the universe could now be observed. In the last few decades the techniques of radio astronomy have been vastly improved and observable wavelengths have been getting shorter, which is technically more difficult. At the same time in optical astronomy the observable wavelengths have been getting longer, extending well into the infrared. It is only in the past twenty years that the area between these wavelengths, the submillimetre region, has been focused on and it is now possible to observe those wavelengths for which radio techniques become very difficult and optical techniques begin to break down. Sometimes this region is also referred to as the *far infrared*.

The continuum emission from dust clouds in the cold interstellar medium (ISM), produced by thermal radiation, can be viewed at submillimetre wavelengths. This emission has quite a broad band spectrum and has the characteristics of blackbody radiation. It therefore follows Wein's displacement law,

$$\lambda_{\max} T = 0.2898 \times 10^{-2}\, mK \qquad (1.1)$$

Thus the emission intensity peaks at a wavelength that is characteristic of the equilibrium temperature T. The temperature of interstellar dust clouds, 10K to 100K [5], is such that the intensity peaks in the submillimetre region. This is of great interest to astronomers as it is from these dust clouds that stars and planets are formed. This occurs when self-gravity overcomes thermal, turbulent and magnetic pressures and causes the cloud to collapse [10]. By observing these clouds at submillimetre wavelengths astronomers can investigate the very early stages of star birth. This continuum emission is most sensitively detected using bolometers, which are devices that simply absorb incident radiation and warm up. This changes their resistance so that when fed with a constant bias current a change in voltage is produced across the device [10]. They are usually held in a liquid helium cryostat at the focus of a large reflector to improve sensitivity to the levels required for doing useful astronomy.

Another type of radiation observed at submillimetre wavelengths has the form of line emission. This is associated with rotational transitions in ions, atoms and molecules with the

emission of photons when these species drop to a lower energy state. By examining the wavelength spectrum of the emitted radiation, astronomers can identify constituent elements of a source, or by measuring the Doppler shift can calculate the corresponding velocity.

Synchrotron radiation is yet another form observed at submillimetre wavelengths. It is caused by streams of particles moving at relativistic speeds through a magnetic field. Matter spiralling towards a black hole generates such emissions as does our own Sun as charged particles are ejected outward through its magnetic field. A group at NUI Maynooth has observed this radiation at sub-100GHz frequencies. Astronomers use synchrotron radiation to detect distant stars from Earth based observatories.

In conclusion, submillimetre astronomy is mainly used to observe the distribution, temperature and motion of dust, atoms and molecules in the universe and the very early stages of star formation in 'stellar nurseries', the dust and gas clouds in the interstellar medium often referred to as 'molecular' clouds. There are many telescopes that have been designed specifically for these observations. The James Clerk Maxwell Telescope (JCMT), the Caltech Submillimetre Observatory (CSO) and the Submillimetre Array (SMA), all of which are located on Mauna Kea at 4000m above sea level in Hawaii, and the Swedish-ESO Submillimetre Telescope (SEST) are all designed specifically for submillimetre wavelengths.

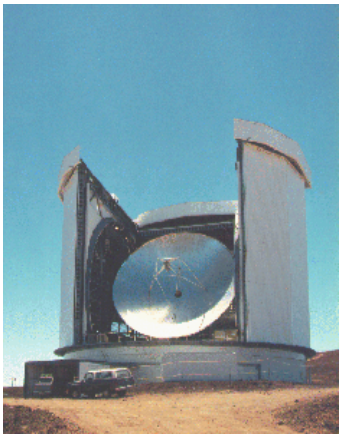

Fig. 1.2: The James Clerk Maxwell Telescope on top of Mauna Kea, Hawaii.

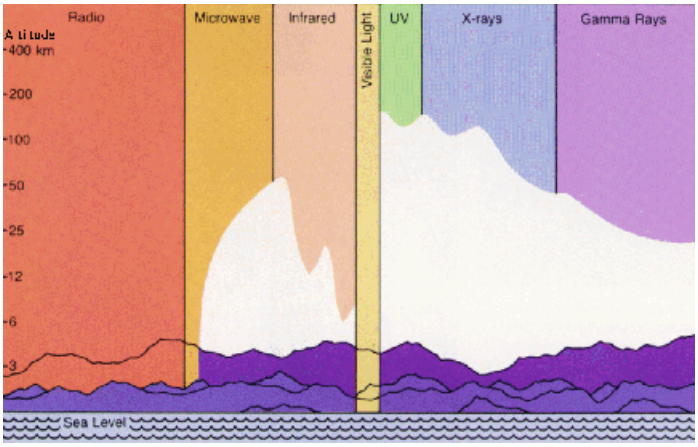

Fig. 1.3: Wavelengths and altitudes at which the atmosphere becomes opaque.

Although ground based observatories are extremely useful, the Earth's atmosphere places limits on the amount of radiation we can detect. Fig. 1.3 shows how the atmosphere is opaque to some wavelengths at different altitudes above sea level. For this reason it is desirable to take measurements as high above the ground as possible. Telescopes and detectors have been

flown in aircraft at very high altitudes and taken up to thirty-five kilometres above ground level in balloons, but the best solution is an orbiting satellite.

The Herschel Space Observatory is one such satellite. This ambitious project by the European Space Agency (ESA) will solve the mystery of how stars and galaxies are born. It will be launched on board an Ariane-5 from French Guiana and will be placed in an orbit at the 2nd Lagrangian point, L2, one and a half million kilometres away from Earth, a distance at which only one other space telescope has previously been placed (MAP arrived there on the 1st October 2001). It will observe wavelengths never comprehensively covered before. The satellite is approximately 7m high and 4.3m wide with a launch mass of around 3.25 tonnes. It will carry the Ritchey-Chrétien telescope, which has a primary mirror with a diameter of 3.5m, the largest satellite IR telescope ever built, and three focal plane experiments:

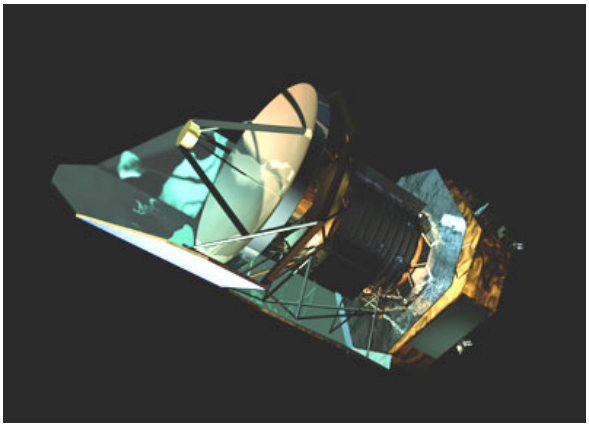

- PACS – *Photoconductor Array Camera and Spectrometer*
- SPIRE – *Spectral and Photometric Imaging Receiver*
- HIFI – *Heterodyne Instrument for the Far Infrared*

Fig. 1.4: An artist's impression of the ESA's Herschel Space Observatory (HSO).

These instruments will be cooled down to below 1K in a cryostat of superfluid liquid helium. This paper is mainly concerned with the science, operation and design of the HIFI instrument on the Herschel Space Observatory.

2. Science with HIFI

HIFI's superb spectral resolution (103 up to 107 or 300 – 0.03Km/s) coupled with its ability to observe thousands of molecular, atomic and ionic lines at submillimetre wavelengths makes it the instrument of choice to probe many of the key questions in modern astrophysics related to the cyclic interaction of stars and the interstellar medium. The instrument combines the high spectral resolving power of the radio heterodyne technique with quantum noise limited detection based on superconducting devices and state-of-the-art microwave technology. This makes it possible to provide continuous coverage from frequencies of

480GHz to 1250GHz in five separate bands. Two additional bands will also observe at 1410GHz to 1910GHz at an unrivalled spectral resolution. The table below (Table 2.1) shows the band number and its corresponding frequency coverage.

Band Number	1	2	3	4	5	6L	6H
Frequency (GHz)	480 – 642	640 – 802	800 – 962	960 – 1122	1120 – 1250	1410 – 1660	1660 – 1910

Table 2.1: Frequency coverage by different bands on HIFI.

One of the major molecules in the universe not observable from ground-based telescopes is H_2O. HIFI will obtain a complete inventory of the most important rotational lines of water and its isotopomers, therefore providing the possibility of tracing the evolution of the water molecule from its origins to its dissociation. The different water lines observed will probe vastly different environments, such as the atmosphere of Mars (Fig. 2.1), and the Orion Molecular Cloud (Fig. 2.2). Since H_2O is the major coolant in star forming regions, HIFI will explore the physics, kinematics and energetics of these regions.

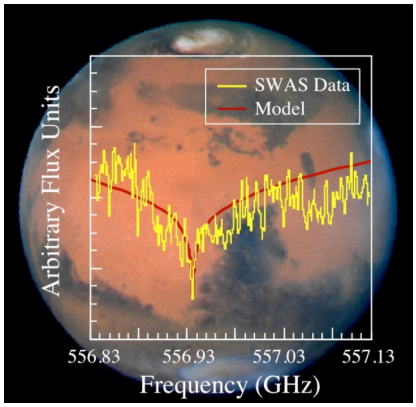

Fig. 2.1: SWAS observations of the 557GHz ground state line of water in the

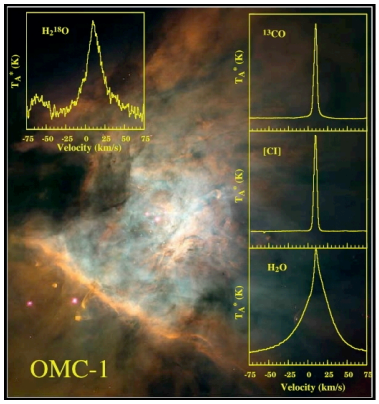

Fig. 2.2: SWAS observations of water Towards a region of high-mass star formation in the Orion Molecular

Apart from H_2O, HIFI will also investigate the origin and evolution of other molecules in the universe. This will be carried out by searching for low-lying ro-vibrational transitions of complex species such as polycyclic aromatic hydrocarbons. A survey of the molecular inventory of diverse regions will also be carried out, including shocked molecular clouds, comet tails, dense Photon-Dominated Regions (PDR's), hot cores and protoplanetary disks around newly formed stars, winds from dying stars and toroids interacting with Active Galactic Nuclei (AGN) engines.

Analysis of the interstellar medium (ISM) will also be undertaken by HIFI. It will measure the mass-loss history of stars from stellar winds and mass outflows which, rather than nuclear burning, dominate the gas and dust mass balance of the ISM, as well as regulating stellar evolution after the main sequence. The pressure of the interstellar gas throughout the Milky Way will also be measured, which will solve the puzzle of the intense galactic [CII] 158μm emission measured by COBE. The ratios of the $^{12}C/^{13}C$ and $^{14}N/^{15}N$ isotopes as a function of galactic radius will be determined for the Milky Way and other galaxies. This will constrain the parameters of the Big Bang and explore the nuclear processes that enrich the ISM.

To understand more about galaxies, HIFI will measure the far-infrared line spectra of nearby galaxies, such as *Centaurus A*, as a template for distant and possibly primordial galaxies. All of this science and astronomy would not be possible were not for the increasing advancement in technology and the use of heterodyne techniques.

3. Quasi-Optical Analysis Using Gaussian Beam Modes

To begin with, it is appropriate to give a brief explanation as to what *quasi-optics* or long wavelength optics actually entails. Quasi-optics deals with the propagation of a beam of radiation that is reasonably well collimated but has relatively small dimensions, transverse to the axis of propagation, when measured in wavelengths [2]. It spans the middle ground between geometrical optics, where the wavelength is assumed to be zero, and diffraction dominated propagation, where the wavelength is approximately equal to the systems dimensions. Quasi-optics therefore includes the situation of a beam of radiation whose diameter is only moderately large when measured in wavelengths.

For different regions of the electromagnetic spectrum, different approaches to understanding the physics involved in propagation are appropriate. Metallic conducting and dielectric waveguides are often used at microwave frequencies to guide the electromagnetic beam, but these structures become lossy at high frequencies because of the materials involved. The power loss per unit length of dielectric materials generally increases at least as fast as proportional to frequency, but loss proportional to the square of frequency is found in the millimetre and submillimetre range [2]. For a rectangular, metallic waveguide, the loss increases as frequency to the power of 1.5. This is where quasi-optics makes its appearance. It takes advantage of the essentially loss-less nature of propagation in free space. Lenses and mirrors are still used for focusing the propagating beam, but they are relatively well separated from each other and are quite thin so that the loss per unit length over which the beam travels is greatly reduced.

One quasi-optical analysis technique is the use of Gaussian beam mode theory, which was developed for the analysis of laser cavities in the 1960's. It was found to be both conceptually and computationally superior to diffraction integral techniques in the analysis of millimetre/submillimetre-wave quasi-optical systems [11]. Consider a monochromatic spatially coherent beam represented by the complex scalar field $E(x,y,z)$. This beam is composed of a linear sum of independently propagating complex modes represented by $\Psi_i(x,y,z)$, of the form,

$$E(x,y,z) = \sum_{0}^{\infty} A_i \Psi_i(x,y,z) \qquad (3.1)$$

where A_i are the mode coefficients and each mode has a transverse amplitude distribution whose envelope is a Gaussian function [7]. The sum of these amplitudes squared is a measure of how good a fit a synthesised beam is to the beam being analysed [4]. The modes are solutions to the wave equation appropriate to quasi-optical propagation.

In the derivation of Gaussian beam modes two important assumptions are made [11]. Firstly, the radiation is assumed to be moving as a paraxial beam whose cross-sectional size is not sufficiently large that it can be treated as an infinite plane parallel wave. By '*paraxial*' we mean that the beam is essentially moving along a given axis but with some diffraction taking place, so the beam spreads out into a small opening angle. Secondly, we assume the radiation can be represented as a scalar field.

The Gaussian beam modes are derived by finding modal solutions to the electric and magnetic wave equations in free space appropriate to paraxial propagation. It is always true that [8],

$$\nabla^2 \mathbf{E} = -\frac{1}{c^2}\frac{\partial^2 \mathbf{E}}{\partial t^2} \qquad (3.2) \qquad\qquad \nabla^2 \mathbf{B} = -\frac{1}{c^2}\frac{\partial^2 \mathbf{B}}{\partial t^2} \qquad (3.3)$$

If the source of the radiation is monochromatic, then the wave equation for the case of the electric field reduces to the Helmholtz equation,

$$\nabla^2 \mathbf{E} = k^2 \mathbf{E} = 0 \qquad (3.4)$$

where, $k = \frac{2\pi f}{c}$ (f is the frequency of the radiation and c is the speed of light). Assuming the electric field may be written in terms of independent scalar distributions $E(x,y,z)$, the three components of the electric field may be treated as scalar versions of the wave equation and therefore Eqn. 3.4 may be written as,

$$\nabla^2 E + k^2 E = 0 \tag{3.5}$$

If a wave is propagating in the *z*-direction then a solution of the form,

$$E = \Psi(x, y, z)\exp(-jkz) \tag{3.6}$$

is appropriate, where $\Psi(x, y, z)$ is a slowly varying function with respect to *z*. If we substitute this into Eqn. 3.5 we get,

$$\frac{\partial^2 \Psi}{\partial x^2} + \frac{\partial^2 \Psi}{\partial y^2} - 2jk\frac{\partial \Psi}{\partial z} = 0 \tag{3.7}$$

or in polar co-ordinates,

$$\frac{1}{r}\frac{\partial}{\partial r}\left(r\frac{\partial \Psi}{\partial r}\right) + \frac{1}{r^2}\left(\frac{\partial^2 \Psi}{\partial \vartheta^2}\right) - 2jk\frac{\partial \Psi}{\partial z} = 0 \tag{3.8}$$

where Ψ varies so slowly with respect to *z* that its second derivative can be neglected (paraxial approximation). The solutions to these equations are a set of modes analogous to the set of modes that characterise the propagation of radiation in a metallic waveguide. The precise nature of the modal solutions depends on the symmetry conditions governing the system and the co-ordinate system chosen [15].

For a system of Cartesian co-ordinates, the solution to this equation is given by a set of modes called *Hermite-Gaussian modes*, which are generally written as,

$$\Psi(x, y) = h_m\left(\frac{\sqrt{2}x}{W}\right)h_n\left(\frac{\sqrt{2}y}{W}\right)\exp\left(\frac{jkr^2}{2R}\right)\exp(j\phi_{mn}) \tag{3.9}$$

where *m* and *n* are transverse mode numbers and r^2 is the radial off-axis distance from the beam centre (i.e. $r^2 = x^2 + y^2$). *R* and *W* are slowly varying functions of *z* and how they evolve with *z* will be discussed further on. ϕ_{mn} is called the '*phase slippage*'. It is mode dependent and is given by the equation,

$$\phi_{mn} = (m + n + 1)\tan^{-1}\left(\frac{\lambda z}{\pi W_o^2}\right) \tag{3.10}$$

where W_o is the beam waist radius. The Hermite-Gaussian beam modes are orthonormal in the sense that,

$$\iint \Psi_{mn}\Psi_{m'n'}dxdy = \delta_{mm'}\delta_{nn'} \tag{3.11}$$

Therefore, for convenience we define the normalised Hermite-Gaussian function to be,

$$h_m(x,W) = \frac{1}{\sqrt{2^{m-0.5}\, m!\sqrt{\pi W^2}}} H_m\left(\frac{\sqrt{2}x}{W}\right)\exp\left(-\frac{x^2}{W^2}\right) \qquad (3.12)$$

where $H_m(\gamma)$ is a Hermite polynomial of order *m* in γ (as defined in Gradsteyn *et al* [3]).

Alternatively, for a system of cylindrical polar co-ordinates, the solution to the wave equation can be written in terms of a set of modes called *Laguerre-Gaussian modes*, which are given by,

$$\Psi^c_{mn}(r,\vartheta,z) = \frac{2}{W\sqrt{\pi}}\left(\frac{2r^2}{W^2}\right)^{\frac{n}{2}} l_n^m\left(\frac{2r^2}{W^2}\right)\cos(m\vartheta)\exp\left(-\frac{r^2}{W^2}\right)\exp\left(-\frac{jkr^2}{2R}\right)\exp(j\phi_{mn}) \qquad (3.13)$$

$$\Psi^s_{mn}(r,\vartheta,z) = \frac{2}{W\sqrt{\pi}}\left(\frac{2r^2}{W^2}\right)^{\frac{n}{2}} l_n^m\left(\frac{2r^2}{W^2}\right)\sin(m\vartheta)\exp\left(-\frac{r^2}{W^2}\right)\exp\left(-\frac{jkr^2}{2R}\right)\exp(j\phi_{mn}) \qquad (3.14)$$

where,

$$l_n^m\left(\frac{2r^2}{W^2}\right) = \left(\frac{(m+n+1)!}{n!}\right)L_n^m\left(\frac{2r^2}{W^2}\right) \qquad (3.15)$$

with $L_n^m(\varepsilon)$ being an associated Laguerre polynomial of order *m* and degree *n* in ε [3]. In this case Ψ^c_{mn} and Ψ^s_{mn} are orthonormal as are the Hermite-Gaussian modes.

For a cylindrically symmetric system the solution to the Laguerre-Gaussian modes can be written as,

$$\Psi_m(r) = \frac{1}{W}\sqrt{\frac{2}{\pi}} l_m^0\left(\frac{2r^2}{W^2}\right)\exp\left(-\frac{r^2}{W^2}\right)\exp\left(-\frac{jkr^2}{2R}\right)\exp(j\phi_m) \qquad (3.16)$$

where $l_m^0(\gamma)$ is a normalised zeroth order Laguerre polynomial of degree *m*. Again we must take into account the phase slippage when propagating the Laguerre-Gaussian modes and this can be written as,

$$\phi_m = (2m+1)\tan^{-1}\left(\frac{\lambda z}{\pi W_o^2}\right) \qquad (3.17)$$

where *z* is the axis of propagation.

For propagation, we consider the fundamental mode of the Hermite-Gaussian mode set. It has a Gaussian profile and is the simplest mathematical solution to the Helmholtz equation. This mode is given by,

$$\Psi_0(x,y) = \frac{1}{W}\sqrt{\frac{2}{\pi}}\exp\left(-\frac{r^2}{W^2}\right)\exp\left(-\frac{jkr^2}{2R}\right) \qquad (3.18)$$

and represents a Gaussian beam propagating in the *z*-direction, whose intensity profile does not change as it propagates except for a re-scaling factor as shown in Fig. 3.1 & Fig. 3.2.

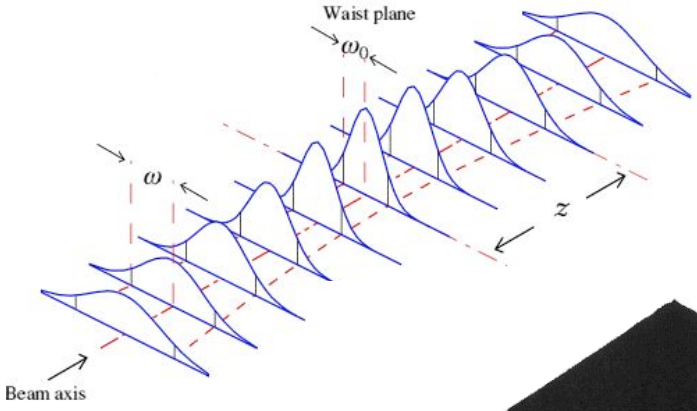

Fig. 3.1: Profile of the fundamental Gaussian as it propagates in free-space.

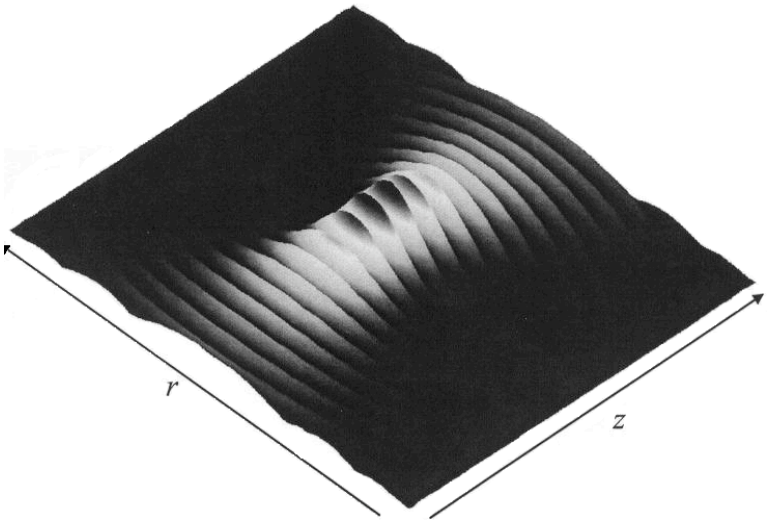

Fig. 3.2: Propagating fundamental Gaussian beam mode showing both the change in width and the radius of curvature.

The off-axis distance at which the amplitude is equal to $1/e$ is given by the beam width parameter, W. This parameter varies as the beam propagates along the *z*-axis and at some distance *z* away from the waist is given by,

$$W^2(z) = W_o^2\left[1+\left(\frac{\lambda z}{\pi W_o^2}\right)^2\right] \qquad (3.19)$$

where W_o is the radius at the waist at which W is a minimum, which is known as the *beam waist radius*.

Another property of the beam that varies as it propagates is called the *phase front radius of curvature*, R, which describes the curvature of the equiphase surface of the beam [15]. The expression for R is written as,

$$R(z) = z\left[1 + \left(\frac{\pi W_o^2}{\lambda z}\right)^2\right] \tag{3.20}$$

At the beam waist, the radius of curvature is infinite and the beam is similar to a plane wave (Fig. 3.3). At a large distance from the waist radius, the radius of curvature is just equal to that distance, so that the beam looks like a spherical wave spreading from a point source at the waist (Fig. 3.4).

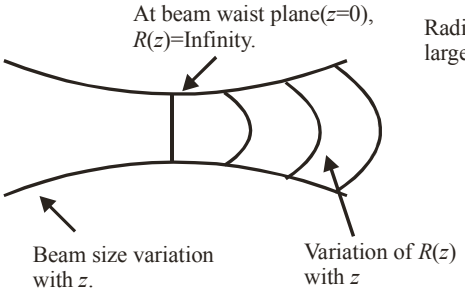

Fig. 3.3: Variation in R(z) as the *beam propagates along the z-axis.*

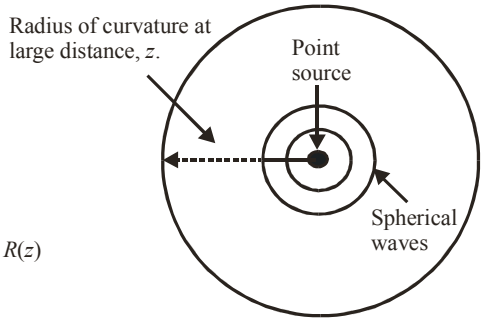

Fig. 3.4: At large values of z, the radius *of curvature has the same value as z.*

When propagating several modes, it is very important to include the effects of the phase slippage. Effectively different modes, Ψ_{mn}, have different phase velocities. If a field consists of a sum of modes, the relative phase between component modes varies along the axis of propagation since the phase slippage term (Eqn. 3.17) is a function of z and is mode number dependant. This results in the amplitude distribution of the composite field altering shape (or form) with z, as in diffraction theory [9].

As an example of the application of Gaussian beam mode analysis we consider the diffraction pattern produced by a straight edge placed in the path of a plane wave, $E(x, y, z) = E_0 \exp(-jkz)$. This can clearly be regarded essentially as a one-dimensional problem. We use a Hermite-Gaussian modal set and consider an expansion of the form [9],

$$E(x,z) = \sum_m A_m h_m(x, W(z)) \exp\left[-jk\left(z + \frac{x^2}{2R(z)}\right) + j\left(m + \frac{1}{2}\right)\tan^{-1}\left(\frac{\lambda z}{\pi W_o^{\,2}}\right)\right] \tag{3.21}$$

In this case the phase slippage term is not incorporated into the amplitude coefficients. If we are only interested in the plane where the obstruction lies, and we are taking this to be the position of the beam waist, then $z = 0$ and the expression reduces to,

$$E(x) = \sum_m A_m h_m(x, W_o) \tag{3.22}$$

where the A_m values are calculated by,

$$A_m = \int_0^\infty f(x) h_m(x, W_o) dx \tag{3.23}$$

letting $f(x) = 1$ for a plane wave. In this case the straight edge is placed at $x = 0$ and lies along the *y*-axis. Depending on the number of modes used to reconstruct the field, the reconstruction will fail beyond a certain value of *x* since modes only reach a finite distance off axis (determined by mode number and *W*). Therefore, it is essential to use the correct number of Hermite-Gaussian modes.

A reconstruction of a field with a waist of 1mm and wavelength of 0.1mm is shown in Fig. 3.5. The field is shown at the plane of a straight edge along the *y*-axis as described above and sixty Hermite-Gaussian modes were used. Clearly because of the finite number of modes used the edge is not a discontinuity. The clear ringing seen is similar to that seen in Fourier

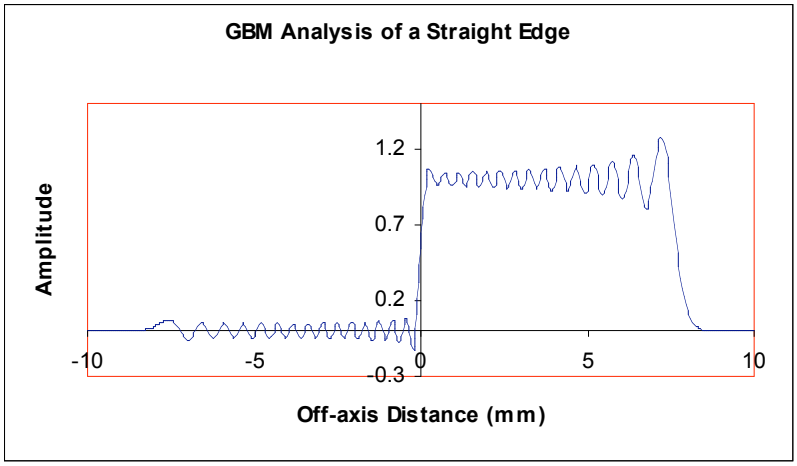

Fig.3.5: Reconstruction of a field at the plane of a straight edge which lies along the y-axis (waist = 1mm, λ = 0.1mm).

Series when reconstructing sharp edges. The ringing period depends on the number of modes used.

Clearly, sharp edges are difficult to reconstruct in any modal approach. However, away from planes where fields are clipped the modal method approaches a very good approximation to the diffracted field. It does underline however, that an appreciation of the limitations of the numerical approach (i.e. only a finite number of modes being used in the modal sum) is

important to any analysis. A similar approach was used to analyse a system of a circular aperture with a stop, analogous to the layout of a Cassegrain telescope, the results of which are shown in Fig. 3.6, Fig. 3.7 and Fig. 3.8. The beam was assumed to have a wavelength, λ, of 1mm and a waist radius of 9mm with one hundred Laguerre-Gaussian modes being used in the reconstruction. The circular aperture had a radius of 10mm and the stop a radius of 2mm.

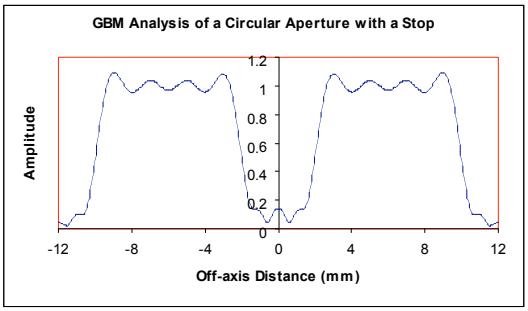

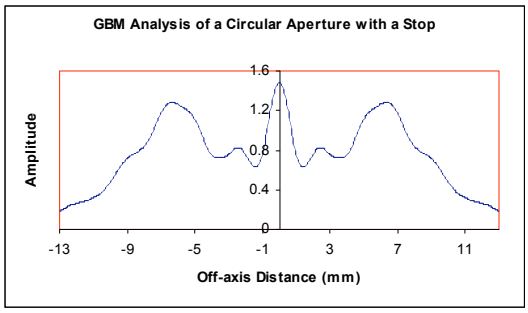

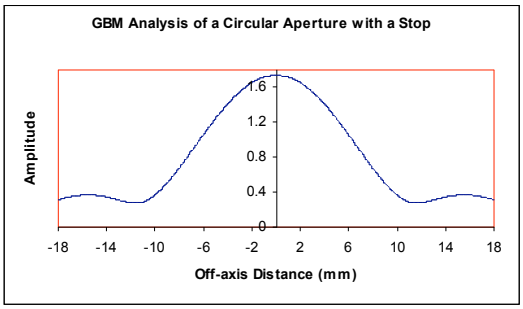

Fig. 3.6 (top left): Reconstruction of the field at the plane of the circular aperture.

Fig. 3.7 (top right): Reconstruction of the field at a distance of 20mm (20λ) from the plane of the circular aperture.

Fig. 3.8 (bottom): Reconstruction of the field at a distance of 200mm (200λ) from the plane of the circular aperture. This is the far field.

In conclusion, both the straight edge and the circular aperture are examples of how Gaussian beam mode analysis proves very useful. We can easily switch from Cartesian co-ordinates, as in the case of the straight edge, to polar co-ordinates for systems with circular symmetry. It is also possible to analyse focussing optical components such as curved mirrors and lenses, which allows Gaussian beam modes to be used in the analysis of a complete optical system.

Other techniques used for quasi-optical analysis include ray tracing, Fresnel diffraction and physical optics. Each method has its own advantages and disadvantages but used together form a powerful set of tools for analysing different properties of the optics in question. For this reason, in the analysis of a complete system, many different methods must be used for a full understanding of the underlying processes. The following sections will show how these techniques of quasi-optical analysis were put to use in the design and analysis of the integrated lens antenna on the HIFI instrument.

4. The Optical Layout of HIFI

Alongside the Herschel Space Observatory inside the launch vehicle will be another satellite called PLANK. Therefore, due to the small size of the Ariane-5 vehicle and the enormous cost of putting satellites into space, the size of the HSO is restricted and therefore so too is the size of the HIFI optics. As the initial optical design was undertaken by TPD (TNO, the Institute of Applied Physics, Delft) using ray tracing and geometrical optics in the limit where $\lambda = 0$, it was crucial to analyse the system more realistically, taking the long wavelength of the submillimetre radiation into account. The geometric analysis is not completely adequate to describe the propagation of beams where diffraction effects need to be considered.

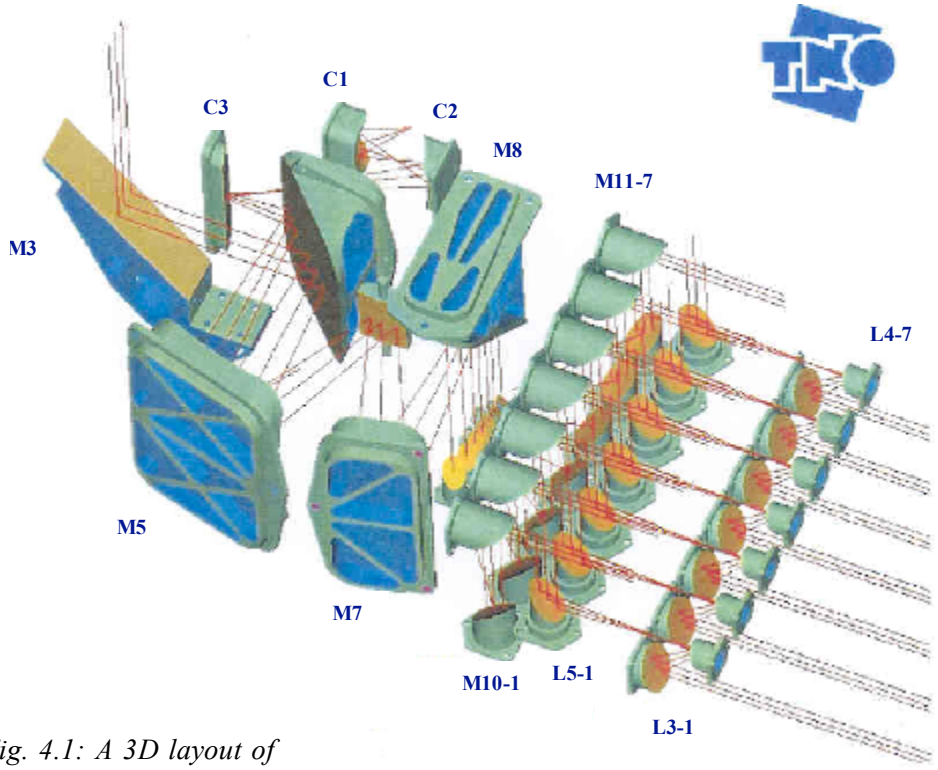

Fig. 4.1: A 3D layout of the HIFI optical system.

This paper is mainly concerned with the integrated lens antenna and mirror system in band 5 of HIFI. Since this band has the lowest frequency of all those channels containing lens antennas, it will suffer more severely from diffraction problems and therefore, if the design can be verified at this wavelength, it can be adapted to the other bands. The full HIFI focal plane optical system consists of a number of distinct subsystems: the Common Optics Assembly (COA), the Local Oscillator (LO) Optics and the Mixer Assembly (MA). The COA is basically a relay system directing radiation to seven different mixer assemblies corresponding to the

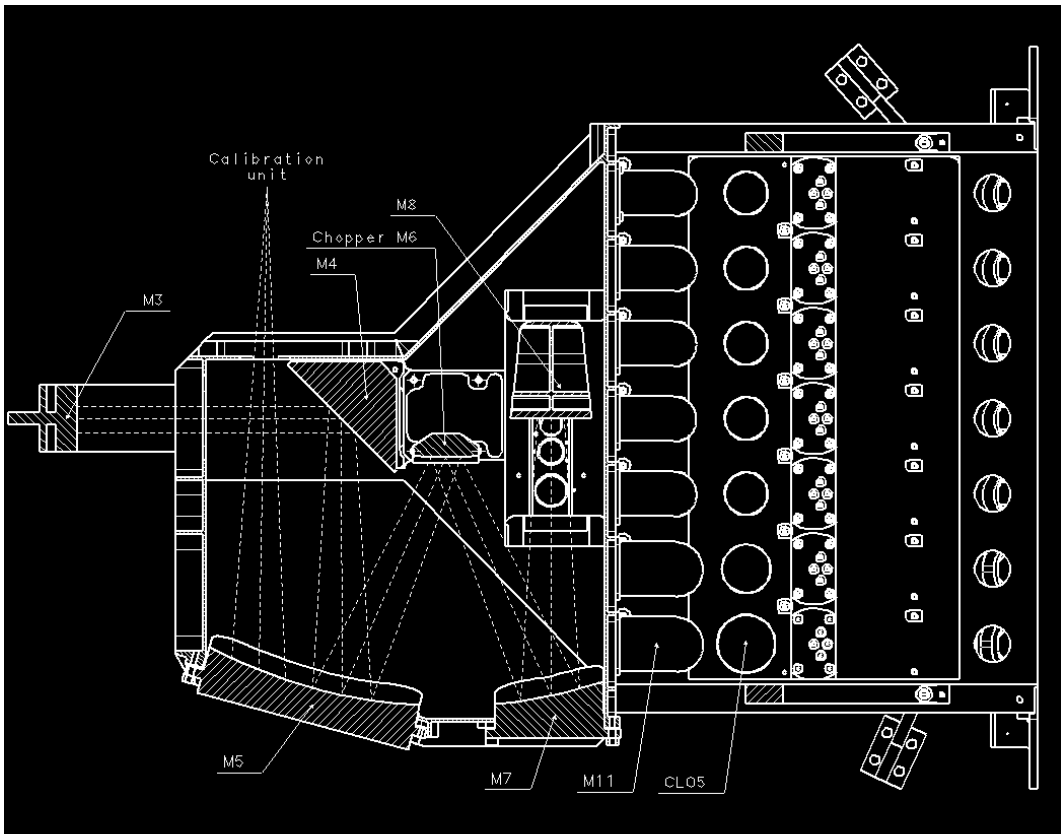

Fig. 4.2: Horizontal cross-section of the common optics and cold LO optics of HIFI

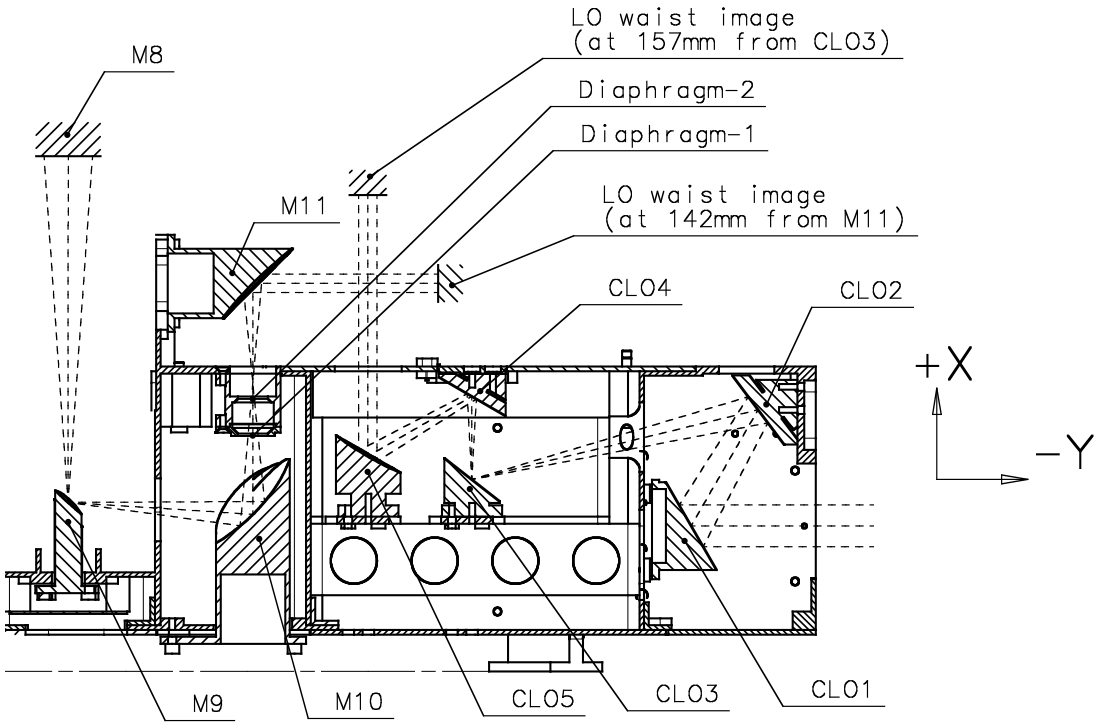

Fig. 4.3: The channel splitting optics and cold LO optics HIFI's channel 4.

channels of HIFI. Within the mixer assemblies (Fig. 4.4), the collimated telescope beam, B CHTEL (Beam Channel TELescope), and the local oscillator beam, B CHLO (Beam Channel Local Oscillator), are coupled and directed to two mixer subassemblies. In channels 5, 6L and 6H, a silicon lens focuses the beam to the submillimetre receiving planar antenna glued to the back surface of the lens.

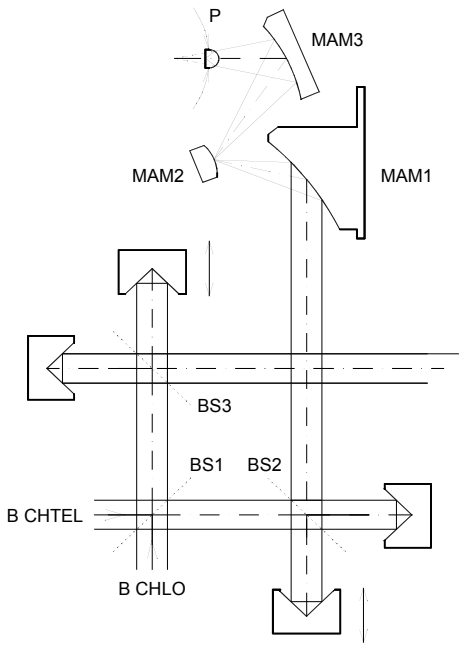

Fig. 4.4: The Mixer Assembly (MA) optics for channels 5, 6L and 6H of HIFI.
Only one mixer subassembly is shown, which consists of mirrors MAM1, MAM2 and MAM3. The beam is then

5. Design and Analysis of the Integrated Lens Antenna

The initial design concept for the integrated lens antenna for band 5 of HIFI was proposed by Caltech (California Institute of Technology). This system consisted of a hyperhemispherical silicon lens with a double-slot feed antenna. The lens had a diameter of 5mm and with a refractive index of 3.14 for silicon, it required an extension length of 0.7316mm using the equation,

$$L_h = \frac{r_S}{\sqrt{\varepsilon_r}} \qquad (5.1)$$

where r_S is the radius of the spherical portion of the lens and ε_r is the relative permittivity of the material. The operating frequency was assumed to be 1185GHz. To reduce reflection losses the lens had a quarter-wavelength matching layer. The double-slot planar feed had a length $l = 77.4\mu m$, a separation of $44.2\mu m$ and the width of the slots was set at $4\mu m$. This

system produces a beam with an f-number of 2.5 or, from Eqn. 5.2, an opening angle of 22.6°.

$$f-number = \frac{f_{eff}}{D_{primary}} = \frac{l_s}{D_{\sec ondary}} = \frac{1}{2\tan\left(\frac{\theta}{2}\right)} \tag{5.2}$$

One problem with this f-number is that because it is quite short, it gives rise to a proportionally small focal spot, causing difficulty in the alignment process of the optical system. Bands 1 to 4 have a have a longer f-number of 4.25. Having the same f-number for band 5 would make for easier testing and would allow the same optical design to be used for all channels. However, by having a longer f-number, the system would suffer from a reduction in the coupling efficiency and an increase in reflection loss at the matching layer and air interface. To investigate this further, two new lens designs were analysed, both of which were elliptical and produced a beam with an f-number of 4.25, which is shown in Table 5.1.

Lens Type	Hyperhemispherical	Elliptical	Elliptical
F-Number	2.5	4.25	4.25
Half Short Axis	2.5mm	2.819mm	2.439mm
Half Long Axis	2.5mm	2.846mm	2.496mm
Diameter	5.0mm	5.638mm	4.878mm
Extension	0.731mm	0.851mm	0.673mm
Matching Layer	Quarter-wavelength	None	None
Lens Name (for referral in paper)	HypHem	Ell#1	Ell#2

Table 5.1: Lens data for a hyperhemispherical lens and two elliptical lenses.

In reality the system will be receiving radiation, however, in its analysis we made use of the Theorem of Reciprocity [6], which allowed it to be treated as a transmitter rather than a receiver. The first step in this procedure was to produce the far field radiation patterns of each of the integrated lens antennas, which was carried out using a program called PILRAP (written by Van der Vorst [13]). This software allows the user to input both the lens and

antenna specifications and then uses ray tracing inside the lens followed by physical optics to generate the far field. The far field patterns for all three lenses are shown below (Fig. 5.1).

Although the far field patterns had the required beam width, it was important to ensure that there was no refocusing of the beam in the near field, which could lead to a mismatch with the optics. To check qualitatively for any such effects a ray tracing analysis of the lens designs was also carried out using a

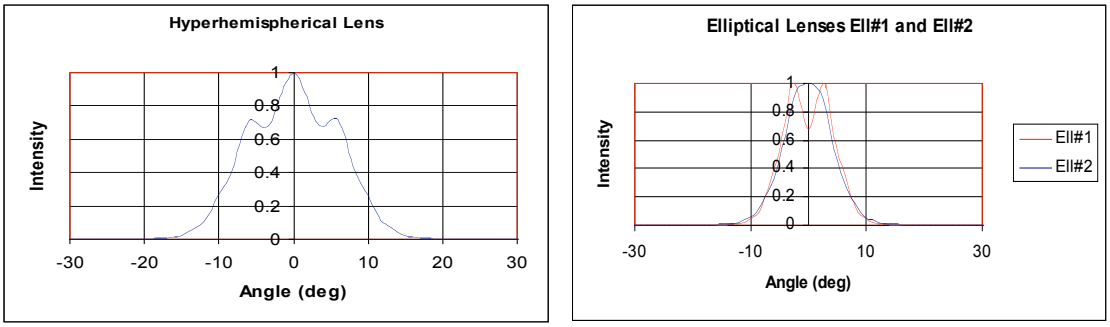

Fig. 5.1: The far field radiation patterns generated by PILRAP for all three lens systems.

commercially available software program called ZEMAX®. This program treats the optical system in question as a system of different 'surfaces' whereby the first is the object surface where the source is located and the final surface is the image surface. For each of these and the surfaces in between, the user may input a 'thickness', a radius of curvature, a conic constant and a material from which the surface, i.e. the component, is made. By giving the surface a radius of curvature and a thickness, the radius of the dielectric lens can be defined, as can the thickness of the extension length. The ray tracing may then be carried out from the object surface to the image plane.

Surface	Type	Radius	Thickness	Glass	Semi-Diameter	Conic Const.
OBJ	STANDARD	0.00E+00	1.00E-05		2.86E-02	0.00E+00
STO	STANDARD	0.00E+00	8.51E-01	SILICON_3.416	2.50E-03	0.00E+00
2	STANDARD	0.00E+00	2.85E+00	SILICON_3.416	2.82E+00	0.00E+00
3	STANDARD	-2.79E-01	2.87E+01		2.82E+00	-1.89E-02
IMA	STANDARD	0.00E+00	0.00E+00		2.97E+00	0.00E+00

Table 5.2: Surface data as defined in ZEMAX for the elliptical lens Ell#1.

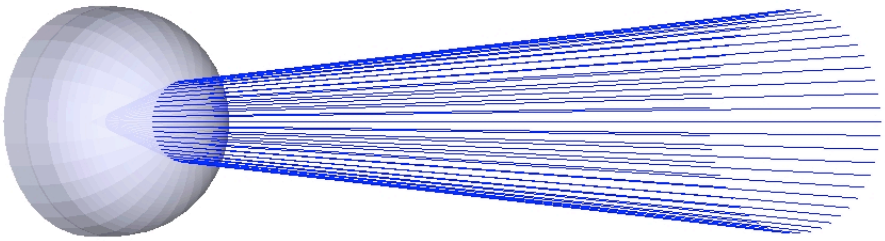

Fig. 5.2: 3D image of the ray tracing analysis carried out on lens Ell#2.

Since the ray tracing showed that there were no unwanted focusing properties (Fig. 5.2) for the three lenses, a Gaussian beam mode analysis was carried out to reproduce the waist field, given the far field pattern from PILRAP. The first step in this is to calculate the Gaussian beam mode coefficients and then synthesise the far field pattern to confirm the results of the calculation. Using the Gaussian beam expansion, the near field can then be produced quite simply. However, there is one subtlety with this approach. The phase front radius of curvature in the far field is not flat with respect to a spherical wave at the PILRAP reference surface in the lens antenna. Thus when the near field is reproduced at the reference surface, it will not be the field at the true beam waist. To overcome this problem, the phase variation in the far field as output by PILRAP was matched to a spherical phase error, which was then subtracted to 'flatten out' the phase. This effectively meant that the new reference plane, with respect to which the beam pattern was calculated, was very close to the true waist position [1]. Both the far field and near field patterns are shown in below as calculated using a Gaussian beam analysis. The total power contained in the fundamental mode, P_0, was also calculated using the equation

$$P_0(in\%) = \left(|A(0)| / \sum_m |A(m)|^2 \right) \times 100 \qquad (5.3)$$

which of course is also a measure of the Gaussicity of the beam. The results of this calculation are shown in the table below.

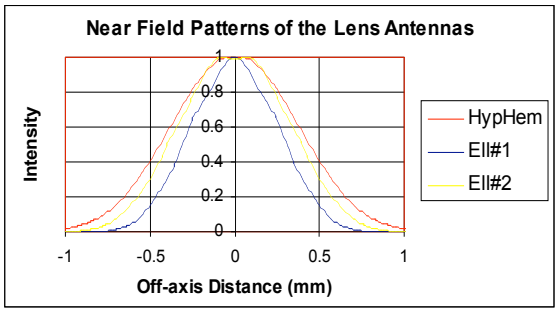

Fig. 5.3: Near field pattern of all three lenses as calculated using Gaussian beam

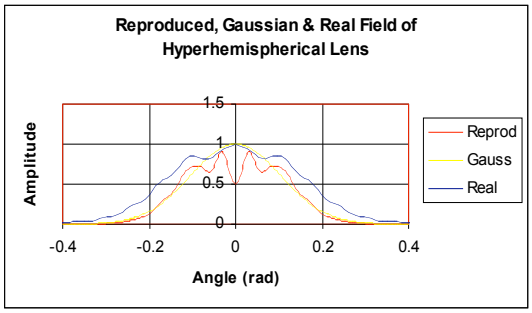

Fig. 5.4: Real far field and reproduced far field of HypHem along with a Gaussian

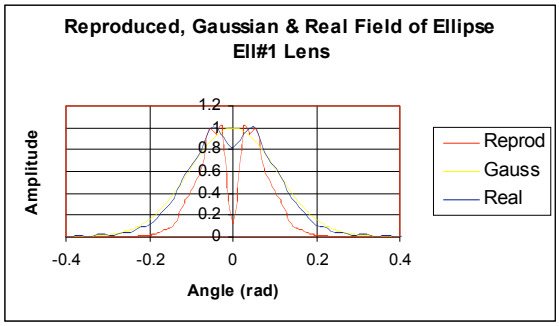

Fig. 5.5: Real far field and reproduced far field of Ell#1 along with a Gaussian

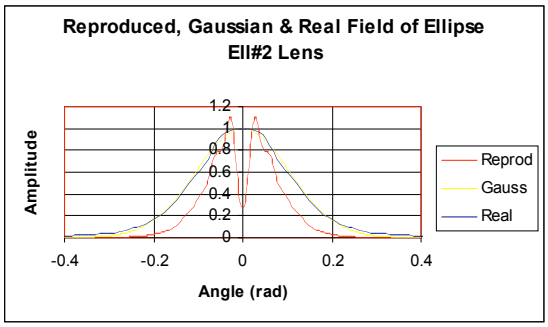

Fig. 5.6: Real far field and reproduced far field of Ell#2 along with a Gaussian

Lens Name	Waist Radius θ_0 (rad)	Power in Fundamental (as % of total power)
HypHem	0.175	87.95
Ell#1	0.130	94.82
Ell#2	0.140	95.4

Table 5.3: The value of θ_0 and the total power in the fundamental mode for each of the lens types.

Having generated the field at the beam waist plane it then had to be propagated through the three mirrors of the mixer subassembly of HIFI's band 5. This was achieved by using a program called GLAD® (General Laser Analysis and Design). Unlike geometrical optical codes, which represent the optical beam as rays, GLAD® represents the optical beam by the complex amplitude of the optical wavefront. However, it is not specifically designed for the submillimetre region of the spectrum and some functions such as calculating aperture

efficiencies and coupling efficiencies are not possible. To propagate the beam, a starting point and arbitrary output plane are entered, as well as the geometrical parameters of the optical system. The components of the system are then modelled in 3D space with the correct orientation and the desired field (in this case the beam waist field calculated earlier) is imported.

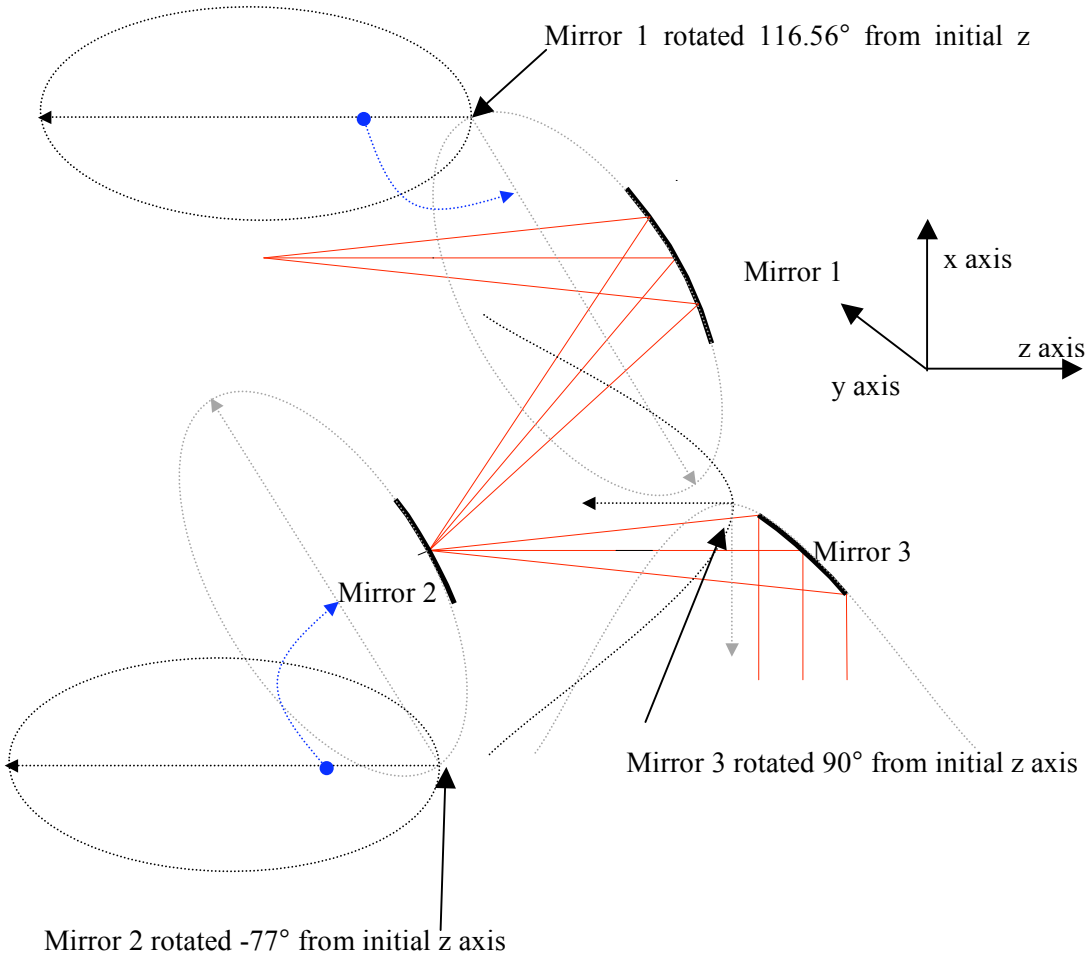

Fig.5.7: Mirror layout of the mixer subassemblv of band 5 as set in GLAD [12].

To compute the telescope aperture efficiency we need to determine the coupling between the telescope signal beam (from the sky), as calculated by N. Trappe [12], with the beam from the lens antenna, having been propagated through the mixer subassembly optics as shown in Fig. 5.8. For two fields, $\sum A_m \psi_m$ and $\sum B_m \psi_m$, which are not normalised, the total fractional power coupling efficiency is calculated by,

$$\eta_{12} = \frac{\left| \sum_m A_m B_m^* \right|}{\sum_m |A_m|^2 \times \sum_b |B_m|^2} \qquad (5.4)$$

This calculation was carried out for the sky beam with the beam from the hyperhemispherical lens and both beams from the elliptical lenses, with and without aberrational effects. The power coupling results are shown in Table 5.4

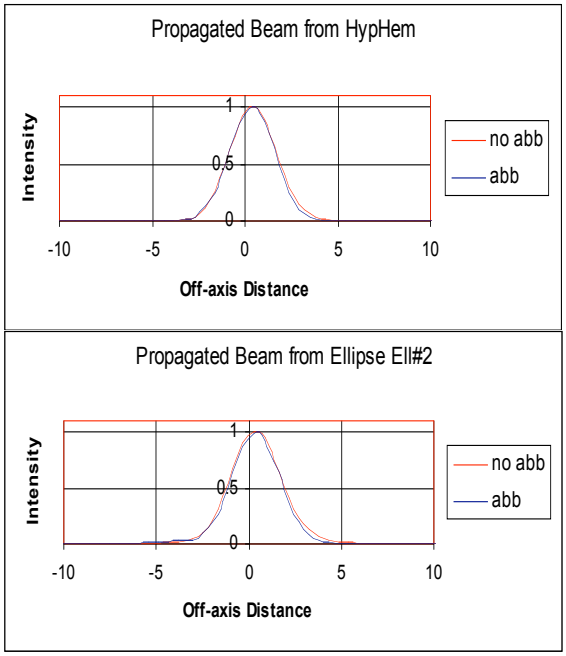

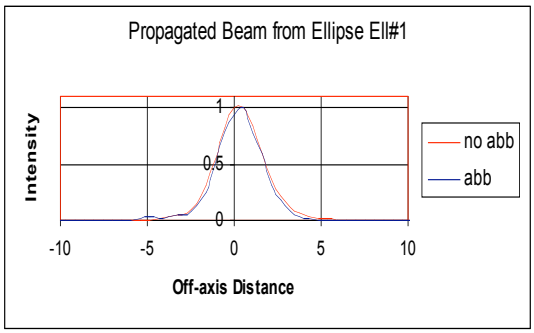

Fig. 5.8: Graphs showing the beams from the hyperhemispherical and two elliptical lens antennas as propagated to the diplexer plane by GLAD. The beams are shown with and without aberration.

Calculated Power Coupling Efficiencies		
	Excluding Aberration %	**Including Aberration %**
HypHem with Sky	80.79	71.59
Ellipse Ell#1 with Sky	77.64	76.40
Ellipse Ell#2 with Sky	74.20	71.68

Table 5.4: Power coupling efficiencies as calculated using Gaussian beam mode coefficients.

6. Conclusion

In this paper we discussed the function of the HIFI instrument on board the Herschel Space Observatory and the astronomy that will be carried out at submillimetre wavelengths. The techniques used in the analysis of quasi-optical systems were discussed with a particular emphasis on Gaussian Beam Mode Theory. These techniques were then applied to the mirror and lens antenna configuration found in HIFI's band 5, with attention given to three different lens designs.

As shown in the previous section, the different lens designs produce beams that couple with different efficiencies to the beam from the sky. In the case of the original hyperhemispherical lens, a coupling efficiency of 80.79% is achieved when neglecting aberration effects. This coupling efficiency is greater than that for either of the other two lens designs, which produce beams with 77.64% and 74.20% efficiency, again neglecting aberration. However, if we examine the efficiency of the beam produced by the elliptical lens Ell#2 and the original hyperhemispherical lens, and take into account the effects of aberration, then clearly there is not much difference between their coupling efficiency values of 71.59% and 71.68% respectively. A difference of 0.9% is obtained, whereas elliptical lens Ell#1 produces a beam with an efficiency of 76.40% (including aberration), yielding a difference of approximately 5% from the other two designs.

This analysis has shown that all three lenses produce beams with quite a high power coupling efficiency. It has also proved that the effects of aberration in the mixer subassembly optical system are large enough not to be neglected, as they will affect the performance of the telescope. Therefore, on choosing a lens design for band 5 of HIFI, it must be noted that it is the elliptical lenses that produce beams with the longer f-number. This was one of the main reasons for changing the original lens design. It can therefore be placed directly into an optical system with the same mirror configuration as the lower frequency bands and will couple as effectively as the lens with the shorter f-number, that is, the original hyperhemispherical lens as proposed by Caltech, in the optical system currently being used in band 5.

Acknowledgements

The work described in this paper was carried out in collaboration with the Submillimetre Space Optics group at the National University of Ireland Maynooth and is ongoing. Other collaborators include ESTEC, SRON and TPD in the Netherlands. A special thanks is extended to Dr. Neil Trappe, Dr. Criéidhe O'Sullivan and Mr. Bill Lanigan. The authors would also like to acknowledge the financial support of Enterprise Ireland and the European Space Agency through a PRODEX award.

References

[1] Curran, G., "*Quasi-Optical Design of the HIFI Instrument for the Herschel Space Observatory*", M.Sc. Thesis, National University of Ireland, Maynooth, Ireland, 2002.

[2] Goldsmith, P.F., "*Quasioptical Systems: Gaussian Beam Quasioptical Propagation and Applications*", IEEE Press, New York, 1998.

[3] Gradshteyn, I.S., Ryzhik, I.M., "*Tables of Integrals, Series and Products*", Academic Press Inc., Orlando, 1980.

[4] Heanue, M., "*Submillimetre-Wave Local Oscillator Multiplexing Using Phase Gratings*", M.Sc. Thesis, St. Patrick's College Maynooth, Ireland, 1995.

[5] Holliday, K., "*Introductory Astronomy*", John Wiley & Sons Inc., Chichester, 1999.

[6] Kraus, J.D., Marhefka, R.J., "*Antennas for All Applications*", Third Edition, McGraw-Hill, New York, 2002.

[7] Lesurf, J.C.G., "*Millimetre-Wave Optics, Devices and Systems*", Institute of Physics Press, 1993.

[8] Martin, D.H., Lesurf, J.C.G., "*Sub-millimetre-wave Optics*", Infrared Physics, **vol. 18**, pp. 405 – 412, 1978.

[9] Murphy, J.A., Egan, A., "*Examples of Fresnel Diffraction Using Gaussian Modes*", Eur. J. Phys., **vol. 14**, pp. 121 – 127, 1993.

[10] Ray, T.P., Beckwith, S.V.W., "*Star Formation and Techniques in Infrared and mm-Wave Astronomy*", EADN Predoctoral Astrophysics School V, Springer-Verlag, 1992.

[11] Siegman, A.E., "*Lasers*", University Science Books, California, 1986.

[12] Trappe, N., "*Quasi-Optical Analysis of the HIFI Instrument for the Herschel Space Observatory*", Ph.D. Thesis, National University of Ireland, Maynooth, Ireland, 2002.

[13] Van der Vorst, M., "*Integrated Lens Antennas for Submillimetre-Wave Applications*", Ph.D. Thesis, Technical University Eindhoven, Netherlands, 1999.

[14] Verschuur, G.L., Kellermann, K., "*Galactic and Extragalactic Radio Astronomy*", Springer-Verlag, New York, 1988.

[15] White, D., "*Computer Aided Design of Sub-Millimetre Wave Quasi-Optical Systems*", M.Sc. Thesis, St. Patrick's College Maynooth, Ireland, 1995.